

Quantum non-Markovianity and localization

David Davalos¹, Carlos Pineda^{1,2}

¹*Instituto de Física, Universidad Nacional Autónoma de México, México D.F. 01000, México and*

²*University of Vienna, Faculty of Physics, Boltzmanngasse 5, 1090 Wien, Austria*

(Dated: March 12, 2022)

We study the behavior of non-Markovianity with respect to the localization of the initial environmental state. The “amount” of non-Markovianity is measured using divisibility and distinguishability as indicators, employing several schemes to construct the measures. The system used is a qubit coupled to an environment modeled by an Ising spin chain kicked by ultra-short pulses of a magnetic field. In the integrable regime, non-Markovianity and localization do not have a simple relation, but as the chaotic regime is approached, simple relations emerge, which we explore in detail. We also study the non-Markovianity measures in the space of the parameters of the spin coherent states and point out that the pattern that appears is robust under the choice of the interaction Hamiltonian but does not have a classical-like phase-space structure.

PACS numbers: 03.65.Yz, 03.67.-a

I. INTRODUCTION

Open quantum systems were recognized as an important subfield of quantum mechanics early in their history [1], because understanding them allows one to explain ubiquitous phenomena, such as spontaneous decay [2]. Later, the Lindblad equation was proposed to describe the evolution of the reduced density matrix of a quantum system weakly coupled to a memoryless environment [3–5]. Environments that lie outside that approximation (Lindblad equation) have attracted the attention of the community in later years. This is, arguably, because we now have such delicate control of quantum systems that memory effects become experimentally relevant [6], and environment engineering is possible [7, 8] to mitigate or even use such effects [6, 9, 10]. A whole community is now dedicated to the study of such systems, known as *non-Markovian* environments. Numerous efforts have been made to define non-Markovianity (NM) in a precise manner, to measure it, and to take advantage of it (see the previous review papers and Refs.[11, 12]). Many systems have been studied under this program, both theoretically and experimentally [6].

Currently, there are many examples of non-Markovian environments that produce a variety of effects. However, not much is known regarding what the key properties that might boost the non-Markovianity of an environment are. Some properties, such as the structure of the phase space of the classical counterpart of the environment have proven to be crucial; however, what happens when we do not find such a classical analog? In this paper we focus on two questions. First, is the value of the several measures of non-Markovianity for long times, only dependent on the effective dimension of the Hilbert space? Second, is there a hidden underlying classical structure in the environment that we can unveil with the help of these measures?

To study these questions, we consider a qubit coupled to a kicked spin chain, which has integrable, mixed and chaotic dynamical regimes [13, 14], but, as far as we

know, no semiclassical analog. The interaction between qubit and environment is set up so as to have dephasing, so all the decoherence effects on the qubit are contained in a suitably defined fidelity of the environment. To quantify NM, we use two commonly used measures [15, 16] and a third that was recently introduced and which has a direct relation with a physical task [11].

We find complex relations between NM and the localization of initial environmental states in the integrable and mixed regimes, which depend on the peculiarities of each NM measure. In fact, in Ref.[17] a relation between localization, induced by disordered, and a particular non-Markovianity measure was explored for an environment consisting of an array of cavities. In the case of the recently introduced measures [11], the effective dimension of the Hilbert space of the environmental states has an important role which leads to more complex behavior. In the chaotic regime, due to the ergodic properties of the Hamiltonian, the relation is simpler and almost homogeneous. Regarding the search for underlying classical structure, we focus our attention on the features that emerge in the space of the parameters of the initial states (spin coherent states) when the NM and the *inverse participation ratio* (IPR) [18] are calculated. We searched for the characteristic finely granulated fractal structure predicted by the Kolmogorov–Arnold–Moser (KAM) theorem but found only a coarse non fractal one.

The paper is organized as follows. In Sec. II we give a brief introduction to the measures used for non-Markovianity and for localization of quantum states. In Sec. III we present the general scheme of dephasing dynamics and the details of the dynamics. In Sec. IV, we present and discuss the results. We finish by summarizing the results in Sec. V.

II. TOOLS

A. Identifying non-Markovianity

Many measures of non-Markovianity have been proposed: The two most wide spread are the BLP (introduced by Breuer, Laine and Piilo in [15]) and RHP (introduced by Rivas, Huelga and Plenio in [16]) measures. The first is based on the violation of the contraction property of Markovian systems, i.e., decreasing distinguishability between initial quantum states. The second is based on the violation of a well known mathematical property of Markovian process, divisibility of the quantum map. Both criteria come from the classical theory of Markovian stochastic process. A whole new set of measures have been proposed [10]. One of these [11], proposed by the authors of this paper, is based on quantifying the probability of successfully performing a certain task.

It is hard to strictly verify if a stochastic system fulfills the classical definition of Markovianity [19], since it depends on the whole history of the stochastic process. An additional caveat for quantum systems is the fact that in order to observe intermediate states of the system, one would have to measure, thus collapsing the wave function and thus also the probability distributions. This leads, among other problems, to violation of Kolmogorov consistency conditions even for closed quantum systems [10].

One can, however, check the necessary conditions for Markovianity that can be easily interpreted from a physical point of view. For example notice that a classical stochastic process (not necessarily Markovian) can be described by a time dependent right stochastic matrix $A(t)$ that maps the initial probability distribution $\vec{p}(t=0)$ to $A(t)\vec{p}(0) = \vec{p}(t)$. Matrices describing the intermediate process, say the map from time t' to $t \geq t' \geq 0$, described by $A_{t,t'} \equiv A_{t,0}A_{t',0}^{-1}$, will also be right stochastic matrices for Markovian processes. We argue that the intermediate process is a valid one, and if $A_{t,t'}$ is right stochastic for all $t \geq t' \geq 0$, the process is said to be divisible. This construction can be extended to the quantum case, replacing the divisibility concept with the *completely positive* map (CP map), which characterizes a valid quantum channel. Given a quantum process $\mathcal{E}_{t,0}$, we shall say that it is CP divisible if the intermediate dynamics

$$\mathcal{E}_{t,t'} \equiv \mathcal{E}_{t,0}\mathcal{E}_{t',0}^{-1}, \quad t \geq t' \geq 0 \quad (1)$$

are CP maps. Figure 1 illustrates the general idea for divisibility and CP divisibility. A general property of a CP divisible process is that given any Hermitian operator Δ the trace norm decreases under the action of the map [9] $\|\mathcal{E}(\Delta)\|_1 \leq \|\Delta\|_1$, where $\|\cdot\|_1$ is the *trace norm*. In particular, choosing $\Delta = 1/2(\varrho_1 - \varrho_2)$ we have

$$D(\mathcal{E}(\varrho_1), \mathcal{E}(\varrho_2)) \leq D(\varrho_1, \varrho_2) \quad (2)$$

where $D(\varrho_1, \varrho_2) = 1/2\|\varrho_1 - \varrho_2\|_1$ is the *trace distance*. This property shows the contraction of the state space

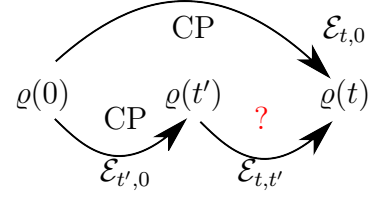


FIG. 1. Illustration of the concept of CP divisibility. The process \mathcal{E} is CP divisible if all existing intermediate maps $\mathcal{E}_{(t,t')}$, are complete positive and trace preserving.

under a Markovian process. This in turn shows how two initial conditions are increasingly forgotten, and are more difficult to distinguish, as the trace norm is directly related with the two state discrimination problem. Some authors *define* Markovianity with this property: If there exists a pair of quantum states such that the last equation does not hold, in Ref. [15] the process is said to be non-Markovian.

B. Quantifying non-Markovianity

Two well-known measures of non-Markovianity can be constructed, based on violations of either Eqs. (1) or (2). In particular, the authors of both measures constructed them adding up the local contributions of the chosen criterion.

For the case of the RHP measure (based on divisibility) the authors define

$$g(t) = \lim_{\epsilon \rightarrow 0^+} \frac{\|\mathcal{J}[\mathcal{E}_{(t+\epsilon,t)}]\|_1 - 1}{\epsilon}, \quad (3)$$

where $\mathcal{J}[\mathcal{E}_{(t+\epsilon,t)}]$ is the Jamiołkowski isomorphism [20] that relates quantum channels and density matrices. In particular, it takes CP maps to positive operators with unit trace. Thus, if $\mathcal{E}_{(t+\epsilon,t)}$ is a CP map, the eigenvalues of the $\mathcal{J}[\mathcal{E}_{(t+\epsilon,t)}]$ will all be positive and add up to one. Otherwise, they will still add up to one, but with negative contributions. Thus, $g(t)$ is greater than zero if at time t the dynamics are not divisible; otherwise, $g(t) = 0$. The measure proposed in Ref. [16] is obtained by integrating the contributions of the non-CP-divisible behavior throughout the entire evolution:

$$\mathcal{N}_{\text{RHP}}[\mathcal{E}] = \int_0^\infty g(t)dt. \quad (4)$$

The brackets here indicate functional dependency.

In a similar spirit, we can integrate the deviations from the contractive behavior, expected for Markovian evolution. Considering the derivative of the trace distance

$$\sigma(t, \varrho_{1,2}(0)) = \frac{dD(\varrho_1(t), \varrho_2(t))}{dt}. \quad (5)$$

According to Eq. (2), $\sigma \leq 0$ for Markovian dynamics. We can integrate this deviation to obtain the measure proposed in Ref. [15], where a maximization over all states

is taken. Thus,

$$\mathcal{N}_{\text{BLP}}[\mathcal{E}] = \max_{\varrho_1, \varrho_2} \int_{\sigma > 0} \sigma(t, \varrho_1(0), \varrho_2(0)) dt. \quad (6)$$

These two measures have some serious drawbacks. In particular, they are not continuous in the spaces of functions, and small fluctuations can change the value of the measure by an arbitrarily large amount. Notice that these issues arise always with a finite Hilbert size environment, and also in finite number statistics. One has the option to cut the integration interval to a finite time, or smooth out the fluctuations by windowing the data. One can also consider other proposals [11] which not only remove that problem, but also provide a physical interpretation for the number obtained. The proposals are

$$\mathcal{N}_K^{\text{max}}[\Lambda_t] = \max_{t_f, \tau \leq t_f} [K(t_f) - K(\tau)] \quad (7)$$

and

$$\mathcal{N}_K^{(\cdot)}[\Lambda_t] = \max \left\{ 0, \max_{t_f} [K(t_f) - \langle K(\tau) \rangle_{\tau < t_f}] \right\}. \quad (8)$$

In this case, K is a quantity associated with the channel and/or its derivative. This can be, say, the quantum capacity, the trace distance with respect to some fixed states, or even $\dot{K}(t) = g(t)$ as defined in Eq. (3).

C. Fidelity and localization

A very simple model of an open quantum system is one in which the dynamics of both the system of interest (central system) and environment are considered and taken to be unitary. If the interaction between them commutes with the Hamiltonian governing the system, one has dephasing dynamics. This kind of dynamics is the simplest decoherence type and is the one considered in this article. If the central system is a qubit, one can write the evolution operator as

$$U = |0\rangle\langle 0| \otimes U_0 + |1\rangle\langle 1| \otimes U_\delta \quad (9)$$

with U_0 and U_δ acting on the environment and $|i\rangle\langle i|$ ($i = 0, 1$) appropriate projectors on the qubit. Given that the initial state of the whole system is the separable state $|\psi_{\text{sys}}\rangle \otimes |\psi_{\text{env}}\rangle$, the dynamics on the qubit only depend on the *fidelity amplitude* [21] defined as

$$f(t) = \langle \psi_{\text{env}} | U_\delta^\dagger(t) U_0(t) | \psi_{\text{env}} \rangle \quad (10)$$

and the expectation value of the echo operator $M(t) = U_\delta^\dagger(t) U_0(t)$ with respect to the state $|\psi_{\text{env}}\rangle$. In particular, the unitary dynamics of the qubit are going to be encoded in the phase of f ; other quantities such as purity, that are invariant under unitary transformations, depend only on the fidelity

$$\mathcal{F}(t) = |f(t)|^2. \quad (11)$$

It follows that in the dephasing scenario, the study of non-Markovianity reduces to the study of the fidelity amplitude in the environment.

If we consider long discrete times, and under ergodic conditions, one can assume that the sequence of states $M(t)|\psi_{\text{env}}\rangle$ is random with respect to $|\psi_{\text{env}}\rangle$; by that we mean that $\langle \psi_{\text{env}} | M(t) | \psi_{\text{env}} \rangle$ is a sequence of random Gaussian numbers. In this model the fidelities are uncorrelated Gaussian random numbers with zero mean and standard deviation inversely proportional to the square root of the dimension of the Hilbert space in which $|\psi_{\text{env}}\rangle$ lives. However, systems that are not ergodic, from a classical point of view, do not explore the whole phase space. The simplest correction to the model proposed leads to the concept of *effective Hilbert space*. The dynamics, for a fixed initial state, can often be described with smaller subset of states sharing a quantum number with the initial state. Say, if the initial state of a semiclassical integrable system lives in a torus, we can describe the evolution with the eigenstates belonging to that same torus. Thus, the dynamics are taking place in an effective Hilbert space of dimension roughly equal to the number of coherent states that cover that torus. In a purely quantum scenario, such a situation arises naturally when one has “good” quantum numbers. A reasonable way to quantify to what extent one can describe states in terms of a small number of states of an orthonormal basis is using the *inverse participation ratio* (IPR). This quantity is defined for a normalized state $|\psi\rangle$ with respect to the orthonormal basis $\{|n\rangle\}$ as

$$\text{P}^{-1}(|\psi\rangle) = \sum_n^{\dim \mathcal{H}} |\langle n | \psi \rangle|^4. \quad (12)$$

The lower bound for the IPR is $1/\dim \mathcal{H}$ and is attained when we have equal weights of $|n\rangle$ on the state $|\psi\rangle$; we say that $|\psi\rangle$ is a fully delocalized state. The upper bound of 1 is obtained by states of the base $\{|n\rangle\}$; we say that $|\psi\rangle$ is localized. Typically the basis $\{|n\rangle\}$ is chosen as the normal eigenbasis of some operator, typically the Hamiltonian prior to a perturbation. It should be noted that such an operator can not have degenerate spectra in order to avoid ambiguities in the basis and get well-defined IPRs.

D. Putting together the tools

At this point, we wish to connect the three quantities discussed: non-Markovianity measures, fidelity, and IPR. Non-Markovianity measures are determined, for dephasing channels, by the fidelity of an environment. In particular, as can be seen from Eqs. (4) and (6), they are determined by the fluctuations of fidelity. In turn, under an ergodic hypothesis, the IPR can tell us how asymptotic fidelity behaves, with an effective dimension yet to be determined. In this paper we want to study under which circumstances we can reduce the study of

non-Markovianity to the study of an effective dimension of a quantum system.

III. MODEL

In this section we start with a generic Hamiltonian that induces dephasing dynamics. We then specify the particular model to be used as environment, namely, a kicked chain of spin-1/2 particles and the initial states of the environment. We complete our model specifying the interactions considered in this work.

A. Dephasing dynamics

The Hamiltonian of a qubit under dephasing dynamics is, up to rotations in the qubit,

$$H = \frac{\Delta}{2} \sigma_z \otimes \mathbb{1} + \mathbb{1} \otimes H_{\text{env}} + \epsilon \sigma_z \otimes V \quad (13)$$

[as in Eq. (9), when writing tensor products, the first term acts on the qubit and the second, on the environment]. The first term is the free Hamiltonian of the qubit and Δ is the transition energy between the two levels; H_{env} is the environmental Hamiltonian; finally, ϵ modulates the coupling strength of the qubit-environment system, provided by the last term. Since the internal Hamiltonian of the qubit commutes with the interaction Hamiltonian we can ignore the latter; it contributes with a unitary transformation in the qubit that does not affect the non-Markovianity measures. The total Hamiltonian can thus be written as

$$H = |0\rangle\langle 0| \otimes H^{(+)} + |1\rangle\langle 1| \otimes H^{(-)}, \quad (14)$$

where $H^{(\pm)} = H_{\text{env}} \pm \epsilon V$; its associate unitary operator takes the form Eq. (9). If we write the channel in the Pauli basis $1/\sqrt{2}\{\mathbb{1}, \sigma_x, \sigma_y, \sigma_z\}$, its matrix elements are given by $\mathcal{E}_{jk} = (1/2)\text{tr}[\sigma_j U(t) \sigma_k \otimes \varrho_{\text{env}} U^\dagger(t)]$, where $|\psi_{\text{env}}\rangle\langle\psi_{\text{env}}|$ is the initial state of the environment and $\sigma_0 \equiv \mathbb{1}$. We arrive to the expression

$$\mathcal{E} = \begin{pmatrix} 1 & 0 & 0 & 0 \\ 0 & \text{Re}[f(t)] & \text{Im}[f(t)] & 0 \\ 0 & \text{Im}[f(t)] & \text{Re}[f(t)] & 0 \\ 0 & 0 & 0 & 1 \end{pmatrix} \quad (15)$$

with f the fidelity of $|\psi_{\text{env}}\rangle$ with respect to the unitary operators $U^+(t) = \exp(-itH^+)$ and $U^-(t) = \exp(-itH^-)$.

For this channel, all measures of non-Markovianity given in the last section can be easily computed and depend only on $F(t) = \sqrt{\mathcal{F}(t)}$. For example,

$$\mathcal{N}_{\text{RHP}}[\mathcal{E}] = \int_{\dot{F}>0} \frac{\dot{F}(t)}{F(t)} dt = \sum_i [\log(F(b_i)) - \log(F(a_i))], \quad (16)$$

with b_i and a_i the times of the i -th maximum and minimum of $F(t)$ respectively. For the computation of the BLP measure, the states that maximize Eq. (6) are those lying on the equator of the Bloch sphere in antipodal positions. The trace distance is the Loschmidt echo, $D(\varrho_1(t), \varrho_2(t)) = F(t)$. From Eq. (6), the measure is

$$\mathcal{N}_{\text{BLP}}[\mathcal{E}] = \int_{\dot{F}>0} \frac{dF(t)}{dt} dt = \sum_i [F(b_i) - F(a_i)], \quad (17)$$

This shows a direct relation with both revivals and fluctuations of the Loschmidt echo of the environmental dynamics. Finally, measures $\mathcal{N}_{\mathcal{K}}^{\text{max}}[\Lambda_t]$ and $\mathcal{N}_{\mathcal{K}}^{(\cdot)}[\Lambda_t]$, as long as they are invariant with respect to unitary operations in the qubit, will depend only on F in the same way that the particular \mathcal{K} chosen depends on F .

B. The environment

The system used as environment is the homogeneous Ising spin-1/2 chain kicked by short pulses of magnetic field. This system was proposed by Prosen to study the relation between ergodicity and fidelity [13, 14]. The Hamiltonian reads

$$H_{\text{env}} = \sum_{i=0}^{N-1} \sigma_i^z \sigma_{i+1}^z + \hat{\delta}(t) \sum_{i=0}^{N-1} b^\perp \sigma_i^x + b^\parallel \sigma_i^z, \quad (18)$$

where $\hat{\delta}(t) = \sum_{n=-\infty}^{\infty} \delta(t-n)$ and $\vec{\sigma}_N \equiv \vec{\sigma}_0$. The first term corresponds to a homogeneous Ising interaction strength; b^\perp and b^\parallel are the perpendicular and parallel components of the magnetic field with respect to the direction of the Ising interaction; finally, $\hat{\delta}(t)$ is a train of Dirac δ s with period 1. This system has three well-known dynamical regimes. For both $b^\perp = 0$ or $b^\parallel = 0$ the chain is integrable [13]. For $b^\parallel = b^\perp \approx \sqrt{2}$ the dynamics is chaotic in the sense of random matrix theory [22]. It follows that the nearest neighbor spacing distribution $P(s)$ of the quasienergies resembles the one of the circular orthogonal ensemble, see the appendix. The third regime is an intermediate one where there is level repulsion but the system is not fully chaotic. The Floquet operator is

$$U = \exp\left(-i \sum_{i=0}^{N-1} b^\perp \sigma_i^x + b^\parallel \sigma_i^z\right) \exp\left(-i \sum_{i=0}^{N-1} \sigma_i^z \sigma_{i+1}^z\right), \quad (19)$$

and the evolution operator for longer times is simply $U(n) = U^n$. This model has the advantage that it can be split in one and two qubit operations, as the terms in each of the exponentials commute with one another, and one can thus express the exponential as a multiplication of exponentials each with only one or two particles involved.

In order to map local features of the non-Markovianity and have initially null correlations in any part of the complete system, we use the spin coherent states as initial

states of the environment. They are invariant under permutations and can be regarded as a macroscopic state.

Coherent states are defined as a coherent displacement of the fiducial state $|J = j; m_z = j\rangle$:

$$|\vartheta, \varphi\rangle = e^{-i\varphi S_z} e^{-i\vartheta S_y} |j; j\rangle = \mathcal{D}_{\vartheta, \varphi}^{(j)} |j; j\rangle, \quad (20)$$

where the total spin is given by $j = N/2$, $\mathcal{D}_{\vartheta, \varphi}^{(j)}$ is the rotation matrix in the subspace of spin j . These states form a complete basis in the symmetric subspace. In fact, one can parametrize these states in a Poincaré sphere, and rewrite

$$|\vartheta, \varphi\rangle = \left(\cos \frac{\vartheta}{2} |0\rangle + \sin \frac{\vartheta}{2} e^{i\varphi} |1\rangle \right)^{\otimes N}. \quad (21)$$

The environmental Hamiltonian is invariant under external rotations: The translation operator, which takes state $\otimes_i |\psi_i\rangle$ to state $\otimes_i |\psi_{i+1}\rangle$, commutes with Eq. (19). This symmetry foliates the Hilbert space in quasi-momentum k subspaces [22]. As the translation symmetry leaves Eq. (20) invariant, such states live in the $k = 0$ subspaces, and as the evolution respects the symmetry, it will remain in such subspace. The calculation of the IPR is thus simply

$$P_{\vartheta, \varphi}^{-1} = \sum_{i=1}^{\dim \mathcal{H}_{k=0}} \left| \langle \phi_i^{(k=0)} | \vartheta, \varphi \rangle \right|^4. \quad (22)$$

C. Interaction operator

We shall study three kinds of couplings (local, global and generic), and look for common trends and differences. Local and generic couplings will break the symmetry of the environment, whereas the global one is chosen to maintain it. We continue by presenting the local perturbations.

As mentioned above, the interaction was chosen to induce a dephasing channel, for sake of simplicity. The operator V appearing in Eq. (13), can be seen as a perturbation operator of the environment dynamics [see Eq. (14)]. For the case of global perturbations, we probed altering either the magnetic field or the Ising interaction between neighbors, which correspond to choosing V as

$$V_b \equiv \delta_1(t) \sum_{i=0}^{N-1} \sigma_i^x, \quad V_J \equiv \sum_{i=0}^{N-1} \sigma_i^z \sigma_{i+1}^z. \quad (23)$$

Analogously, for the local interaction of the qubit with the environment, we chose the coupling as

$$V_{0,1} \equiv \sigma_0^z \sigma_1^z, \quad V_0 \equiv \delta_1(t) \sigma_0^x, \quad (24)$$

where only two and one qubits of the environment, respectively, interact directly with the central qubit. Finally, to study the generic case, we consider the simplest choice, inspired in ergodicity arguments of quantum

chaos [23]. We select V from one of the classical ensembles, namely the Gaussian unitary ensemble (GUE). We shall denote that case as V_{GUE} , and it corresponds to a global and structureless perturbation.

IV. RESULTS

The unitary dynamics in qubit plus environment [defined by Eqs. (13) and (18) and the interactions discussed in Sec. III C] induce a specific dephasing channel Eq. (15) once the initial state of the environment is specified. In our case, such state is a coherent state Eq. (20), specified by the parameters ϑ and φ . The environment, a spin chain, will be used in integrable, mixed and chaotic regimes, varying $b^\perp = 0.1, 1$ and 1.4 respectively while fixing $b^\parallel = 1.4$. We use $b^\perp = 0.1$ instead of 0 for integrable dynamics, in order to avoid degeneracies in the spectrum and have a well defined IPR. Corresponding spectral statistics are presented in the appendix. For all calculations, we chose the coupling parameter $\epsilon = 0.1$.

We performed numerical calculations of the measures of NM using time cutoffs of $t_{\text{cut}} = 10^4$ and a mesh in coherent state parameters (ϑ, φ) of $\Delta\vartheta = \Delta\varphi = 0.1$; the two measures Eqs. (4) and Eq. (6) were slightly modified to accommodate to the intrinsic discrete time structure of Eq. (18). We also considered a time cutoff in the integrals of the measures, as the fluctuations caused by a finite dimensional environment would send the aforementioned measures to infinity. The IPR of the initial environmental states were calculated with respect to the eigenbasis of U^+ for simplicity. Since we are taking a small ϵ , the IPR does not vary considerably if instead of U^+ , we consider U^- or a Floquet operator with an intermediate ϵ .

We discuss first the relation of the different measures of NM with respect to the IPR. Next we study the dependence of these quantities with respect to the choice of the state of the environment; that is, we study the structure of the environment that can be seen, studying the decoherence of the qubit. The section is closed with some comments on the generality of the results when one varies the dimension of the environment and the total evolution time considered.

A. Dependence of non-Markovianity on the state localization

We study the behavior of NM, using \mathcal{N}_{RHP} and \mathcal{N}_{BLP} in Sec. IV A 1 and then using $\mathcal{N}_{\mathcal{K}}^{\text{max}}$ and $\mathcal{N}_{\mathcal{K}}^{(\cdot)}$ in Sec. IV A 2, with \mathcal{K} being \mathcal{D} or \mathcal{G} . In the first section, we focus in the cases which the coupling is via global and local nearest neighbor Ising interaction, V_J and $V_{0,1}$ respectively; and a global V_{GUE} operator. In the second section, we focus only on global V_J and V_{GUE} . These interactions represent well what happens for the other cases for each study.

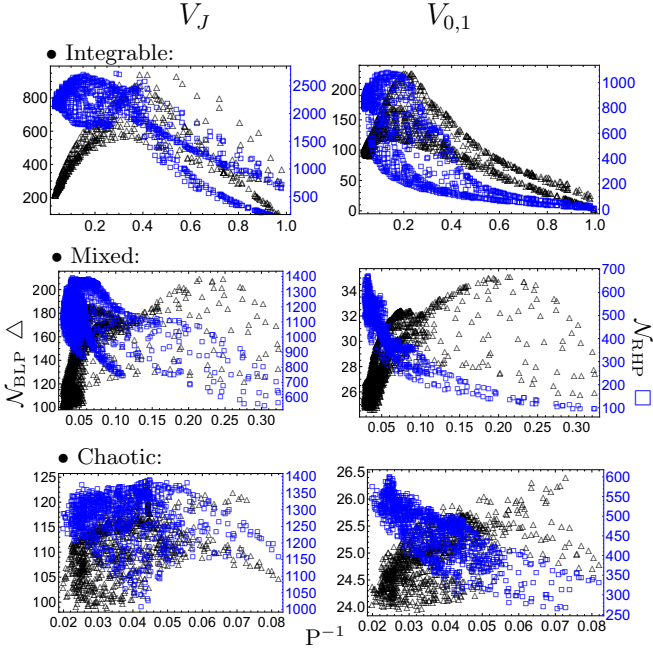


FIG. 2. BLP (black triangles, left axis) and RHP (blue squares, right axis) measures as a function of the IPR for initial coherent states of the environment, Eq. (20), distributed uniformly on the Poincaré sphere. Each column corresponds to a different kind of coupling of the qubit to the environment [see eqs. (23) and (24)], whereas different rows correspond to different dynamical regimes of the environment. The parameters used for this and the rest of the figures are indicated at the beginning of Sec. IV. The results for the global and local field perturbation, V_b and V_0 respectively, are very similar to their global and local Ising counterparts.

1. Using BLP and RHP measures

In Fig. 2 we show, for different initial conditions of the environment and a coupling of the type V_J , the value of NM using BLP and RHP measures as a function of the IPR.

In the integrable regime the two measures have different behaviors; \mathcal{N}_{BLP} grows for increasing IPR until it reaches a maximum around $P^{-1} \sim 0.4$, where it starts to decrease. \mathcal{N}_{RHP} has an approximate monotonic decreasing behavior, showing a change of slope around $P^{-1} \sim 0.4$ and another close to $P^{-1} \sim 0.6$. A local coupling, namely $V_{0,1}$, yields similar results; however, the peak in the BLP measure is sharper and the decay of RHP measure is faster (Fig. 2 second column). The behavior of \mathcal{N}_{BLP} can be explained qualitatively by studying the fidelity which, for the dephasing case, is related to the distinguishability via the equation $\mathcal{D}(t) = |f(t)|^2$. In Fig. 3 we show its evolution in the integrable regime, for three initial conditions and two different environment sizes. For high and low values of localization, oscillations of $\mathcal{D}(t)$ are constrained around high and low values of asymptotic fidelity, respectively. Therefore, the relatively low values of non-Markovianity belong to the high and low

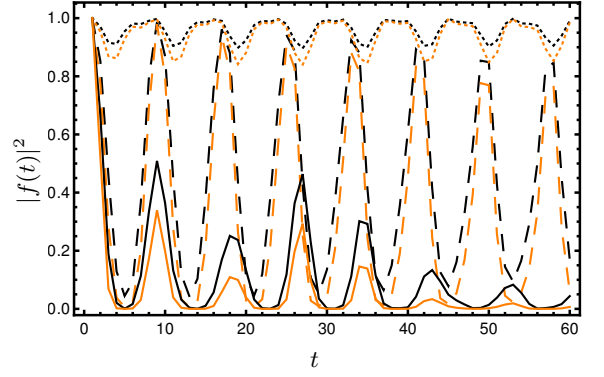


FIG. 3. Typical behavior of the fidelities of the environment, Eq. (18), in the integrable regime with a global Ising perturbation V_J , for several coherent states Eq. (20). We consider 10 and 16 qubits, shown in black and orange curves respectively. The figure shows the fidelity for the state $|\vartheta = 2.8, \varphi = 4.8\rangle$ (with IPR equal to 0.457 and 0.375 for 10 and 16 qubits respectively) which is among the states that yield larger values for measures based on $\mathcal{D}(t)$ (dashed curves). Fidelities for the states that give low values of the BLP measure are the dotted and solid curves, obtained from the states $|\vartheta = 3.0, \varphi = 2.2\rangle$ (IPR equal to 0.994, 0.984) and $|\vartheta = 1.5, \varphi = 3.5\rangle$ (IPR equal to 0.046, 0.010), respectively, which are high and low localized states.

values of localization. There are also states with high IPR that lead to distinguishabilities that oscillate with large amplitude but at a low frequency; those states have low asymptotic fidelity. The maximum value of NM is achieved at ~ 0.4 , where fidelity can oscillate with a large amplitude. One can understand the behavior of \mathcal{N}_{RHP} with similar arguments [see Eq. (16)] but this time taking into account the role of the logarithm. For high localized states the typical values of the minimums and maximums of $\mathcal{D}(t)$ are very close to one or with lower frequency, yielding very small values of the logarithm and thus low values of the RHP measure. As the IPR decreases, the minimums in $\mathcal{D}(t)$ diminishes faster than the maximums, and one reaches quickly the regime in which $-\log(F(a_i)) \sim \mathcal{O}(1)$, causing an increasing of the measure until $P^{-1} \sim 0.4$. For small values of the localization, the typical minimum is very close to zero, for which the logarithm is large, in absolute value. One can approximate $\mathcal{N}_{\text{RHP}} \approx \sum_i \log(F(b_i)) + n \log(F(\tilde{a}^{-1}))$, where n is the number of minimums included in the interval of the computation of the measure and $F(\tilde{a})$ is its typical value. The value of the measure is now seen to be directly related with the localization giving again a monotonic behavior with different slope. For both measures, low localized states tend to cluster. These states are localized in the equator of the Poincaré sphere (see Fig. 9). This explains the two leaf-like structures connected by a stem in the integrable regime.

In the mixed and chaotic regimes fidelities begin with a fast decay after which they fluctuate around the inverse of the effective dimension of the state (Fig. 4). Since the

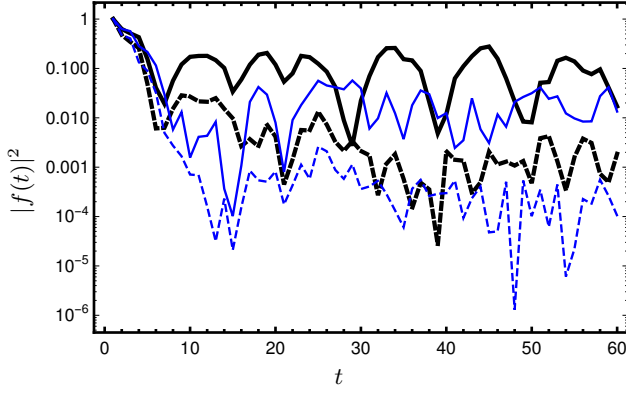


FIG. 4. Typical behavior of the fidelities of the environment in the chaotic (blue curves) and mixed (black thick curves) regimes for 10 (solid curves) and 16 (dashed curves) qubits, with the coupling $V = V_J$; the initial state is a coherent state characterized by $|\vartheta = 0.7, \varphi = 0.8\rangle$, see Eq. (20). A fast decay and fluctuations around a value determined by the effective dimension of the Hilbert spaces, explains the values of the different measures of non-Markovianity.

asymptotic fidelity is inversely proportional to the effective dimension of Hilbert space, the scale of the NM is lower in these regimes with respect to the integrable. The IPR is also small due to ergodic properties of the Hamiltonian. In the mixed regime the slope of the data using V_J and $V_{0,1}$ is positive for BLP measure, while for RHP it is clearly decreasing for both perturbations, mimicking the integrable cases. Thus, both measures behave differently also in the mixed regime. In the chaotic regime, we expect full ergodic properties, and consequently, a similar reasoning to that of the mixed case will follow, however with smaller IPR. Indeed, all initial conditions cluster around a smaller region but a slope, consistent with the mixed cases, is observed.

Finally, we show the results when a random potential provides the coupling in Eq. (13); namely, when we take $V = V_{\text{GUE}}$. The dependence of NM on the IPR is shown in Fig. 5 for both the integrable and the chaotic cases. Its behavior is qualitatively similar to the one observed for the other couplings, when comparing among integrable cases, mixed and chaotic ones. However, there are some quantitative differences. For example, the BLP measure still has an initial growth but is very short compared with the case of $V = V_J$. The same arguments as before can be stated to explain the general features of the behavior.

2. Using measure schemes $\mathcal{N}_{\mathcal{K}}^{\max}$ and $\mathcal{N}_{\mathcal{K}}^{(\cdot)}$

In the previous section we considered measures BLP and RHP, which are based on the non monotonicity of distinguishability, as measured by $\mathcal{D}(t)$, and of divisibility, as measured by $\mathcal{G}(t) = \int_0^t g(\tau) d\tau$. In this section we use measures based on the same quantities, but use

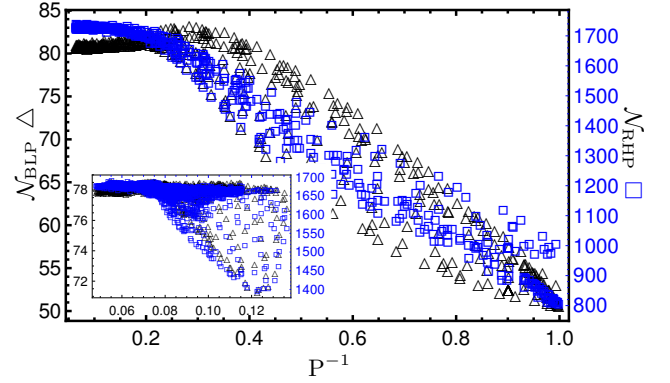


FIG. 5. RHP and BLP measures of the spin chain using a random coupling, chosen from the GUE, in the integrable regime (main panel) and the chaotic regime (inset). We observe a monotonic decreasing behavior for both measures in all regimes, with a short growth for BLP measure in the integrable regime.

Eqs. (7) and (8) to obtain a quantity that can be directly related to a physical process [11], and contrast its behavior with measures BLP and RHP.

For the integrable case, we observe that there are two distinct behaviors, for both measures $\mathcal{N}_{\mathcal{K}}^{\max}$ and $\mathcal{N}_{\mathcal{K}}^{(\cdot)}$, regardless of whether they are based on \mathcal{D} or $\mathcal{G}(t)$. In Fig. 6, we show the results for the case in which the coupling is V_J . These two different behaviors are associated with the two hemispheres of the Poincaré sphere, and its details can be understood by studying the evolution of fidelity. In particular, for $\mathcal{N}_{\mathcal{D}}^{\max}$, one of the branches displays a maximum ($P^{-1} \sim 0.4$), then it decays linearly. The other branch, corresponding to the southern hemisphere ($\pi/2 < \vartheta \leq \pi$), has a slight increase with IPR. The behavior of $\mathcal{N}_{\mathcal{D}}^{(\cdot)}$ is similar; however, it is scaled down, and instead of a slight increase, the southern hemisphere displays a small increase with IPR. A quantitatively similar behavior is seen when we base our measures in $\mathcal{G}(t)$, with the bending point being again at $P^{-1} \sim 0.4$, for $\mathcal{N}_{\mathcal{G}}^{\max}$. $\mathcal{N}_{\mathcal{G}}^{(\cdot)}$ is also a scaled down and slightly deformed version of $\mathcal{N}_{\mathcal{D}}^{(\cdot)}$. For low localized states, the explanation of the aforementioned behavior is similar to the one given for BLP and RHP measures. Since the size of the fluctuations of the fidelity depend on the effective dimension of the state, $\mathcal{N}_{\mathcal{K}}^{(\cdot)}$ and $\mathcal{N}_{\mathcal{K}}^{\max}$ increase as we take more localized initial environmental states. For highly localized states in the integrable regime, there are two families of states. One, with asymptotic fidelity greater than 1/2 and whose fidelity has a high frequency, but small amplitude, and other with asymptotic fidelity smaller than 1/2 but with a fidelity that has smaller frequency and a larger oscillation amplitude. Since the schemes under discussion depend mainly in the amplitude of the oscillations, they are critically sensitive to the asymptotic fidelity of the environmental states. This feature is a significant difference between the newly proposed schemes [11] and the

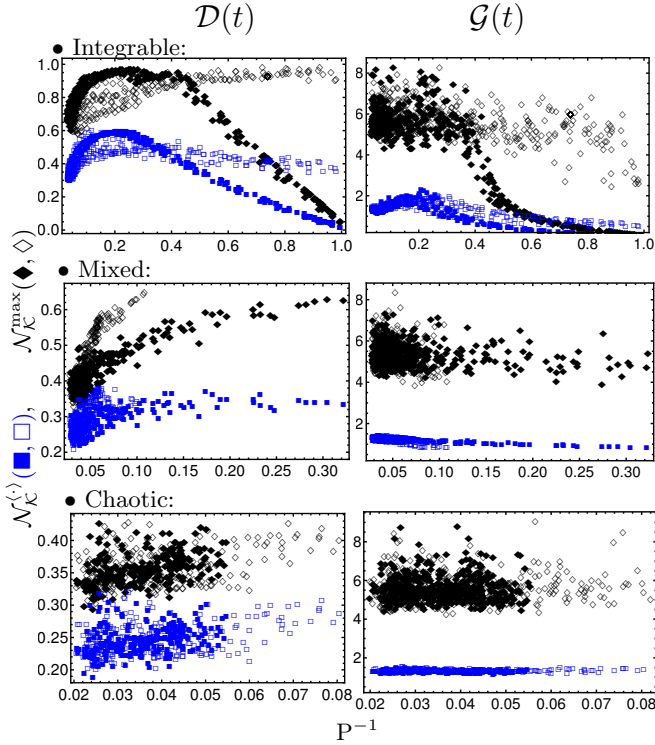


FIG. 6. Measures $\mathcal{N}_K^{(\cdot)}$ (blue) and \mathcal{N}_K^{\max} (black) with $\mathcal{D}(t)$ [left column] and $\mathcal{G}(t)$ [right column], for the spin chain using global Ising perturbation V_J , as a function of the initial IPR of the environment, see Fig. 2. The initial states of the environment are coherent states uniformly chosen from the northern/southern hemisphere of the Poincaré sphere and indicated by the hollow and filled markers, respectively. In the integrable regime (and in the mixed for \mathcal{N}_D^{\max}) we see two different behaviors, coming from the two hemispheres of the Poincaré sphere. The results for local Ising interaction, $V_{0,1}$, are very similar to the presented here. Results for global and local field perturbations, V_b and V_0 respectively, presented only the behavior plotted by filled markers.

more often used BLP and RHP.

In the mixed and chaotic regimes, the behavior of the measures is monotonically increasing. Since all coherent states have a small IPR, the same arguments given before for low localized states in the integrable regime hold to explain such monotonicity. For the chaotic regime the measures also tend to homogenize; this is expected given that the initial states have similar effective dimension, as they appear random in the eigenbasis of the Floquet operator.

For a random coupling to the environment, measures $\mathcal{N}_D^{\max,(\cdot)}$ have a monotonic behavior with respect to IPR. However, in contrast to the behavior of the BLP measure, non-Markovianity increases with the inverse participation ratio. This surprising change can be explained when noticing that the BLP measure depends on the number of pairs of minima and maxima that appear in the fidelity in a given interval, while $\mathcal{N}_D^{\max,(\cdot)}$ depend *only* on the amplitude of the fluctuations of $F(t)$. As we take more

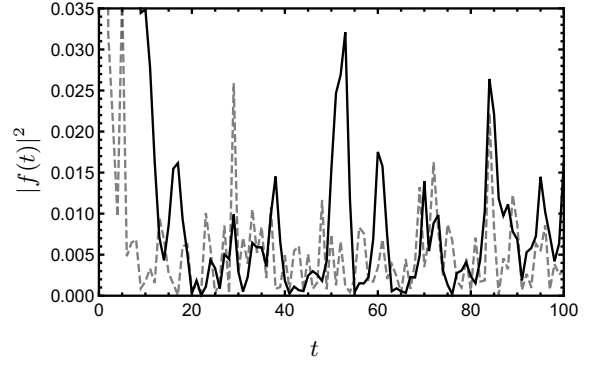


FIG. 7. Typical behavior of the fidelities in the integrable regime for $V = V_{\text{GUE}}$. In solid black we plot the fidelity of the state $|\vartheta = 3.2, \varphi = 1.1\rangle$ as a representative state of highly localized states, and $|\vartheta = 2.2, \varphi = 2.4\rangle$ in dashed gray as a representative of low localized states. High localized states lead to a low frequency of occurrence of pairs of local minima and maxima, while for localized states such frequency is increased. This explains the different behaviors among BLP and $\mathcal{N}_D^{\max,(\cdot)}$.

localized initial environmental states, the size of the fluctuations is increased as the pairs of minima and maxima appear less frequently (shown in Fig. 7), which explains the aforementioned effect. The behavior in the mixed regime, which is also monotonic increasing, has the same explanation. In the chaotic regime the values of NM also tend to homogenize, having the same explanation as the one given for $V = V_J$ for this regime. Now using $\mathcal{G}(t)$ as indicator, all measure schemes in all regimes yield almost constant NM with respect to the IPR (right panels of Fig. 8). This behavior is expected for the chaotic regime; what remains to be explained is its emergence in the integrable and mixed regimes. To do this we can find an upper bound for the change of \mathcal{N}_G^{\max} in the whole interval of localization; we shall call this $\Delta\mathcal{N}_G$. From Eq. (7), $\mathcal{N}_G^{\max} = \log(F(t_f)) - \log(F(\tau))$, where t_f and τ are the maximum and the minimum attained to the maximization required by the definition. Now, since the logarithm is a monotonic function, the measure \mathcal{N}_D^{\max} is attained to the same times, allowing us to write $\mathcal{N}_G^{\max} = \log(\mathcal{N}_D^{\max} + F(\tau)) - \log(F(\tau)) \approx \log(\mathcal{N}_D^{\max}) + F(\tau)/\mathcal{N}_D^{\max} - \log(F(\tau))$. Therefore the total change is $\Delta\mathcal{N}_G = \Delta\log(\mathcal{N}_D^{\max}) + \Delta(F(\tau)/\mathcal{N}_D^{\max}) - \Delta\log(F(\tau))$. The last term can be ignored since $F(\tau)$ is typically very similar for any value of localization. The second term is negative since \mathcal{N}_D^{\max} changes faster than $F(\tau)$ and its absolute value is smaller than the first term which is positive. Therefore $\Delta\mathcal{N}_G^{\max}$ is upper bounded by $\Delta\log(\mathcal{N}_D^{\max})$ and its numerical values for the integrable and mixed regime are 0.4 and 0.08 respectively. There is a similar explanation for $\mathcal{N}_G^{(\cdot)}$ using typical values of the average instead of the minima.

We finish this section by summarizing the results and commenting on practical consequences of the relations we found between non-Markovianity and IPR. The inte-

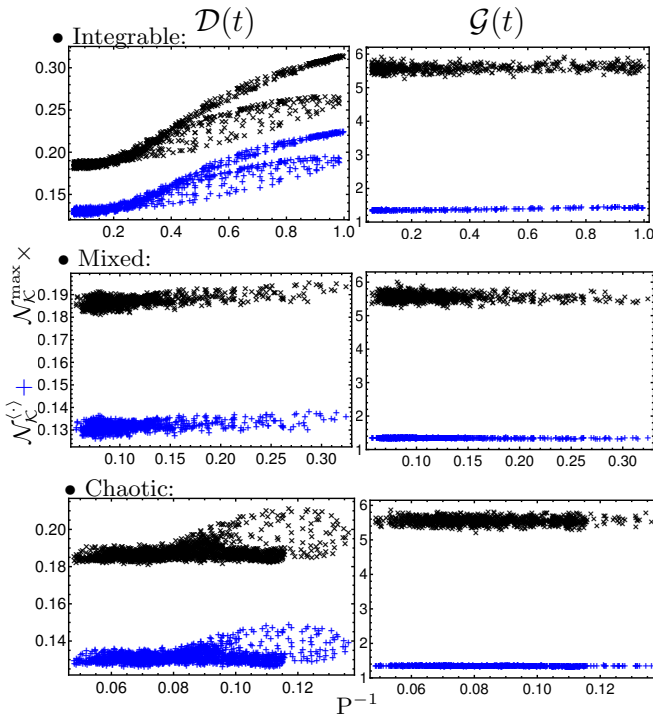


FIG. 8. Relation between $\mathcal{N}_K^{(\cdot)}$ and \mathcal{N}_K^{\max} with IPR, using a global random perturbation. We consider the two measures, based on both $\mathcal{D}(t)$ and $\mathcal{G}(t)$ and a spin chain of eight spins for an ensemble of 40 matrices. Measures based on \mathcal{G} are almost constant in all regimes. For $\mathcal{N}_D^{\max,(\cdot)}$ in the integrable regime, we observe different behaviors for each hemisphere of the Poincaré sphere.

grable regime shows the richest behavior when we use a structured coupling to the environment. In our case we observed a wide variety which includes up to two different behaviors for the two hemispheres of the Poincaré sphere. In general the different measures behave differently and depend on the details of the fidelity. However, the IPR determines coarsely the value of the non-Markovianity. As mentioned in Sec. II B, measure $\mathcal{N}_D^{(\cdot)}$ is directly related to the task of storing information safely; we can see that to perform such a task with a high probability of success, we need an environment in the integrable regime, a structured interaction, and states with intermediate localization. When the environment is in the chaotic regime, the behavior is not so rich, as the coherent states are quite delocalized, and the non-Markovianity seems to be self averaging. In the mixed regime of the environment, we have an intermediate behavior.

B. Underlying structure

In Ref. [24], the authors show that non-Markovianity, via long time fluctuations of fidelity, is able to resolve complex phase space structures of the environment using initial coherent states. In particular, the fractal nature of

the phase space is clearly visible in the mixed regime. We investigated the spin chain in a similar way, using spin coherent states as initial environmental states, studying now the measures of NM and the IPR as functions of the parameters of the spin coherent states. Our goal is to study the visible structures and how they change during the transition from integrability to chaos.

In the integrable regime (top of Fig. 9), the values of the NM measures mimic the behavior of the IPR close to the equator of the Poincaré sphere ($\vartheta = \pi/2$); close to the poles the situation is different. The equator of the Poincaré sphere corresponds to low localized states, and this in turn leads to local minimums for all examined measures of NM. When moving toward the poles, which are very localized states, one finds a local maximum, and then in the vicinity of the pole, a local minimum, for all cases except for \mathcal{N}_D^{\max} near the north pole. The difference arises from the different asymptotic fidelities of the chosen high localized states. This picture deepens the understanding of the behavior already seen in Figs. 2 and 6.

For the mixed regime, the features on the NM measures are mainly governed by the IPR. High localization leads to local maximums in the measure \mathcal{N}_D^{\max} and local minimums for the RHP measure. For the BLP measure, there is also an interesting feature. The local maximum of IPR, located around $\vartheta \approx \varphi \approx 2.5$, leads to a local minimum on the NM which is partially surrounded by a maximum. This behavior is actually similar to the one at the poles in the integrable regime. In the chaotic regime the relation of the measures with the localization practically vanishes.

Regarding the transition from integrability to chaos, using the BLP and RHP measures, there is not a notable change in the size of the structures as it does for environments with a classical analog [24, 25]. This might be due to the absence of such structures, or, that simply due to the relative size of the coherent states in this system, they are not able to resolve small structures. More quantitatively, the fluctuations of the spin coherent states in the Poincaré sphere (chosen to have radius one) scale as $\sim N^{-1}$ [26] i.e. as $[\log_2(\dim \mathcal{H})]^{-1}$, while for coherent states in the torus fluctuations scale as $(\dim \mathcal{H})^{-1}$ [27].

The situation is different when using \mathcal{N}_D^{\max} . In the transition to chaos, a finer structure emerges. Although such features do not appear classical, in the sense of the appearance and breaking of KAM tori, it is clear that there is a finer granularity than is typically expected in this transition; these structures are robust with respect to changes in parameters and times of integration. We consider this one of the central results of this work.

Let us now comment on the results using $V = V_{\text{RMT}}$, shown in Fig. 10. In the integrable regime, measures \mathcal{N}_D^{\max} and $\mathcal{N}_G^{(\cdot)}$ completely mimic the behavior of the IPR, while the BLP measure is anticorrelated with the IPR. Such behavior is a consequence of the way fidelity contributes to the different measures. Recall that the BLP measure depends mainly on the frequency with

which the pairs of minima and maxima occur in $\mathcal{D}(t)$, while schemes $\mathcal{N}_{\mathcal{K}}^{\max}$ and $\mathcal{N}_{\mathcal{K}}^{(\cdot)}$ depend mainly on the amplitude. In the mixed and chaotic regimes the situation is similar: The IPR is correlated with $\mathcal{N}_{\mathcal{D}}^{\max}$ and anti-correlated with BLP. However, for $\mathcal{N}_{\mathcal{G}}^{(\cdot)}$ the landscapes appear to have almost no correlation with IPR.

It is also important to underline that the measures $\mathcal{N}_{\mathcal{G}}^{(\cdot)}$ and $\mathcal{N}_{\mathcal{D}}^{\max}$ show a non-fractal structure in the transition to chaos, as in the results using V_J .

Results using RHP measure are very similar to the ones for BLP; the ones for $\mathcal{N}_{\mathcal{D}}^{(\cdot)}$ resemble the ones for $\mathcal{N}_{\mathcal{D}}^{\max}$, and the results using $\mathcal{N}_{\mathcal{G}}^{\max}$ reveal only a random landscape for all regimes.

C. Generality of the results

This section is devoted to a discussion the validity of the main results presented above for a larger number of qubits and for different cutoff times.

We first discuss three key features, namely (i) the decreasing behavior of the BLP and RHP measures for high localized states (shown in Figs. 2 and 5); (ii) the same property for measures $\mathcal{N}_{\mathcal{K}}^{\max}$ and $\mathcal{N}_{\mathcal{K}}^{(\cdot)}$, but only for the hemisphere which contains the states with low asymptotic fidelity (Fig. 6); and (iii) the peculiar behavior of measures based on $\mathcal{D}(t)$ (also shown in Fig. 6), which exhibits a clear change on the slope as localization is increased. Let us now comment how these observations behave as the dimension of the environment is increased, and for sake of brevity only for measures $\mathcal{N}_{\mathcal{K}}^{\max}$ (shown in Fig. 12). The results show that the patterns are preserved; however, as the dimension increases the data becomes diffused, i.e. for each value of IPR there is a wider range of NM. This is due to the relation between asymptotic fidelity $\overline{\mathcal{F}(t)}$ and IPR (shown in top panel of Fig. 11), which is linear (for each hemisphere of the Poincaré sphere) but spreads out for a larger number of qubits.

It is interesting that this observation also reveals the origin of the above mentioned splitting of the relation between localization and non-Markovianity, due to the different values of asymptotic fidelities of high localized states. Therefore, by plotting the relation of NM versus $\overline{\mathcal{F}(t)}$ (shown in the bottom panel of Fig. 12), it can be seen that the splitting and the spreading of the data are removed, revealing that the relation of NM is simpler as a function of the effective dimension of the Hilbert space of the initial states.

Next, we shall study the emergent structures in the computed measures for the system with a higher dimension (we used a spin chain with 16 qubits). It yields basically the same behavior as for the 10 qubits case (shown in Fig. 13), but there is an emergence of smaller finer features in the landscapes of measure $\mathcal{N}_{\mathcal{D}}^{\max}$ ($\mathcal{N}_{\mathcal{G}}^{(\cdot)}$), which has basically an identical landscape. We conclude that such fine structures become smaller as the dimension is

increased. A general characteristic of the landscapes, especially in the integrable and mixed regimes, is that the local maximums in the IPR determines the most visible structures in the NM. They appear as local maximums or minimums depending on the chosen measure and/or in the asymptotic averaged fidelity of the coherent states of the region.

We finalize this section by discussing the validity of our observations for other cutoff times. In Fig. Fig. 14, we show the values of all the measures treated in this paper for the integrable case and for one state of the environment, as a function of the cutoff time. Measures BLP and RHP are normalized by t_{cut} to avoid their trivial linear dependence. The figure shows that all measures saturate quickly to its asymptotic value, except $\mathcal{N}_{\mathcal{G}}^{\max}$, which saturates more slowly than others but more quickly with respect to the system size. We discussed only the results for one state in one regime since the exploration for other cases gives very similar results.

V. CONCLUSIONS

We performed numerical calculations of the non-Markovianity of a qubit coupled to an environment modeled by a unitary kicked spin chain in a coherent state. Several dynamical regimes of the chain, couplings between qubit and environment, and measures of non-Markovianity, were considered. Additionally, the inverse participation ratio of the environment (with respect to the coupled environment) was calculated.

We explored the relation of NM versus IPR and showed that the schemes $\mathcal{N}_{\mathcal{K}}^{\max}$ and $\mathcal{N}_{\mathcal{K}}^{(\cdot)}$, proposed in Ref. [11] have important and potentially useful differences with respect to the more common measures BLP and RHP. We showed that that the first mentioned schemes reveal the asymptotic fidelity of the environmental state, leading to two clearly different behaviors of the measures in function of the IPR. Regarding the validity of the former results, we showed that the relations between non-Markovianity and localization for larger environments remain the same. However, self averaging was not observed. A central result of the paper is the identification of a maximum of the NM for intermediately localized environmental states, when using distinguishability as indicator. Such a scenario could be used to protect classical information more efficiently [11].

In the second part of the work we presented a study of the NM and the IPR as functions of the parameters of the Poincaré sphere in which the initial coherent environmental states live. We concluded that there are structures mainly depicted by the IPR in all dynamical regimes; these are robust under the election of the interaction Hamiltonian and the dimension of the environment. We have shown that although such structures are not classical-like (in the sense that they do not present KAM behavior), they become finer in the transition to chaos when using measures $\mathcal{N}_{\mathcal{D}}^{\max}$ and $\mathcal{N}_{\mathcal{D}}^{(\cdot)}$. Such fea-

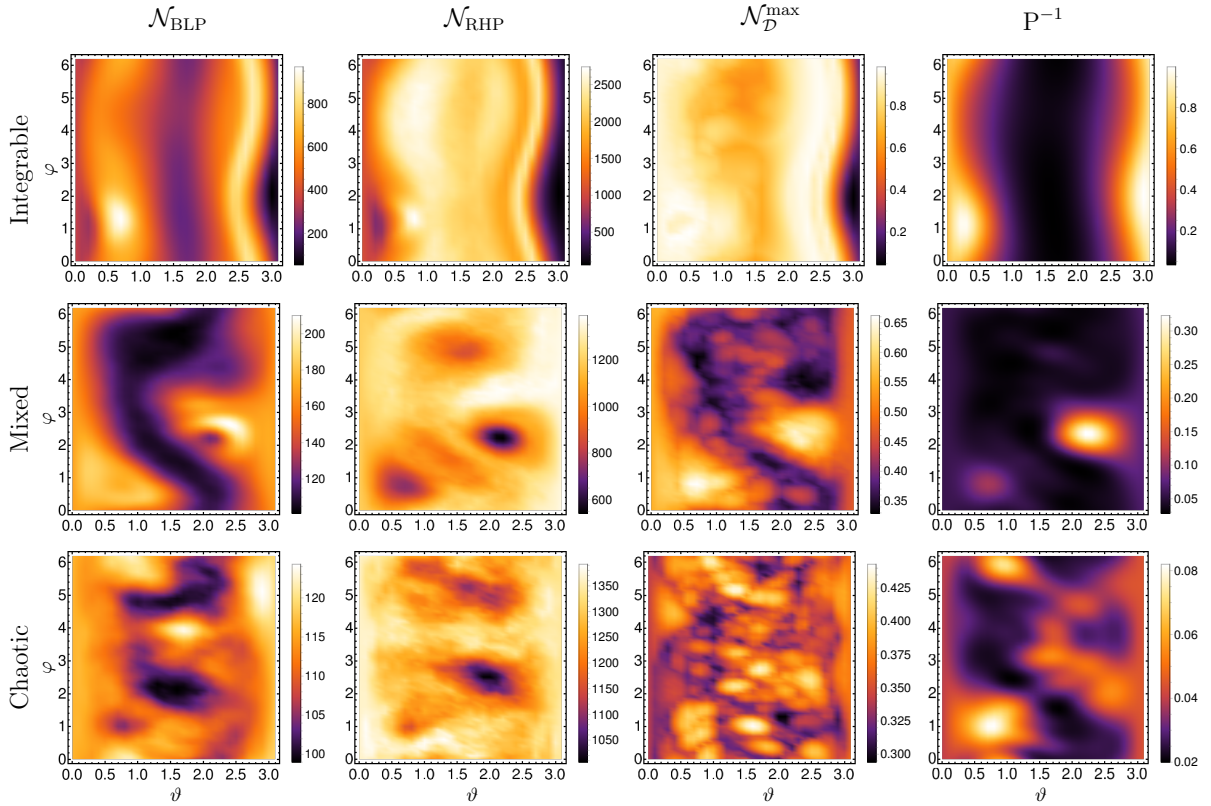


FIG. 9. The different columns correspond to density plots of several measures of non-Markovianity and the IPR, for a chain with 10 qubits using the homogeneous perturbation V_J . For N_D^{\max} some smaller structures appear as we go into the chaotic regime. We can also observe a relation in the integrable and mixed regimes between IPR and all non-Markovianity measures. The results for local Ising interaction, $V_{0,1}$, are very similar, just with more extended depressions. The results for the global and local field perturbations, V_b and V_0 respectively, are very similar to their global and local Ising counterparts.

tures remain stable with respect to the cutoff time, indicating that they are not random fluctuations, and become finer as the dimension increases.

ACKNOWLEDGMENTS

We acknowledge the support by CONACyT and DGAPA-IN-111015, as well useful discussions with Heinz-Peter Breuer, Diego Wisniacki and Thomas Gorin.

Appendix: Dynamical regimes

The spin chain has well known dynamical regimes in the sense of random matrix theory. The analysis of the spectra (the eigenphases of the Floquet operator) has been done for the chaotic regime and for 16 qubits in Ref. [22].

In this appendix we present a brief analysis for the integrable regime for 12 qubits and for completeness also for the chaotic and mixed regimes, following the aforementioned work. In order to show the correspondence of the eigenphases of the Floquet operator with the re-

sults of random matrix theory, we have to identify the subspaces corresponding to the good quantum numbers of the system. We then compute the distribution of the distance among the nearest neighbor eigenphases [named $P(s)$] in each symmetry sector. The homogeneous spin chain has a symmetry under translation of spins, i.e. the Hamiltonian remains invariant if we take the spin i to $i + 1$. Thus we will use the eigenspectra corresponding to the eigenspaces of the translation operator T for the analysis of $P(s)$.

The symmetry operator acts in the computational basis $|\alpha_0, \dots, \alpha_{N-1}\rangle$ ($\alpha_j \in \{0, 1\}$), as $T|\alpha_0, \dots, \alpha_{N-1}\rangle = |\alpha_{N-1}, \alpha_0, \dots, \alpha_{N-2}\rangle$. Since $T^N = \mathbb{I}$, its eigenvalues are simply $\exp(2\pi i k/N)$ with k an integer between 0 and $N-1$. Therefore, the Hilbert space is foliated into N subspaces $\mathcal{H} = \bigoplus_{k \in \mathbb{Z}/N} \mathcal{H}_k$. The chain also has a reflection symmetry given the symmetry operator R , which transforms $R|\alpha_0, \dots, \alpha_{N-1}\rangle = |\alpha_{N-1}, \dots, \alpha_0\rangle$. This symmetry commutes with the T in the subspace identified by $k = 0$, and for even N , also in $k = N/2$; for simplicity these subspaces are removed from the calculation. Figure 15 shows the averaged nearest neighbor spacing distribution over the relevant subspaces, and the ansatz corresponding to the different dynamical regimes [28]. For

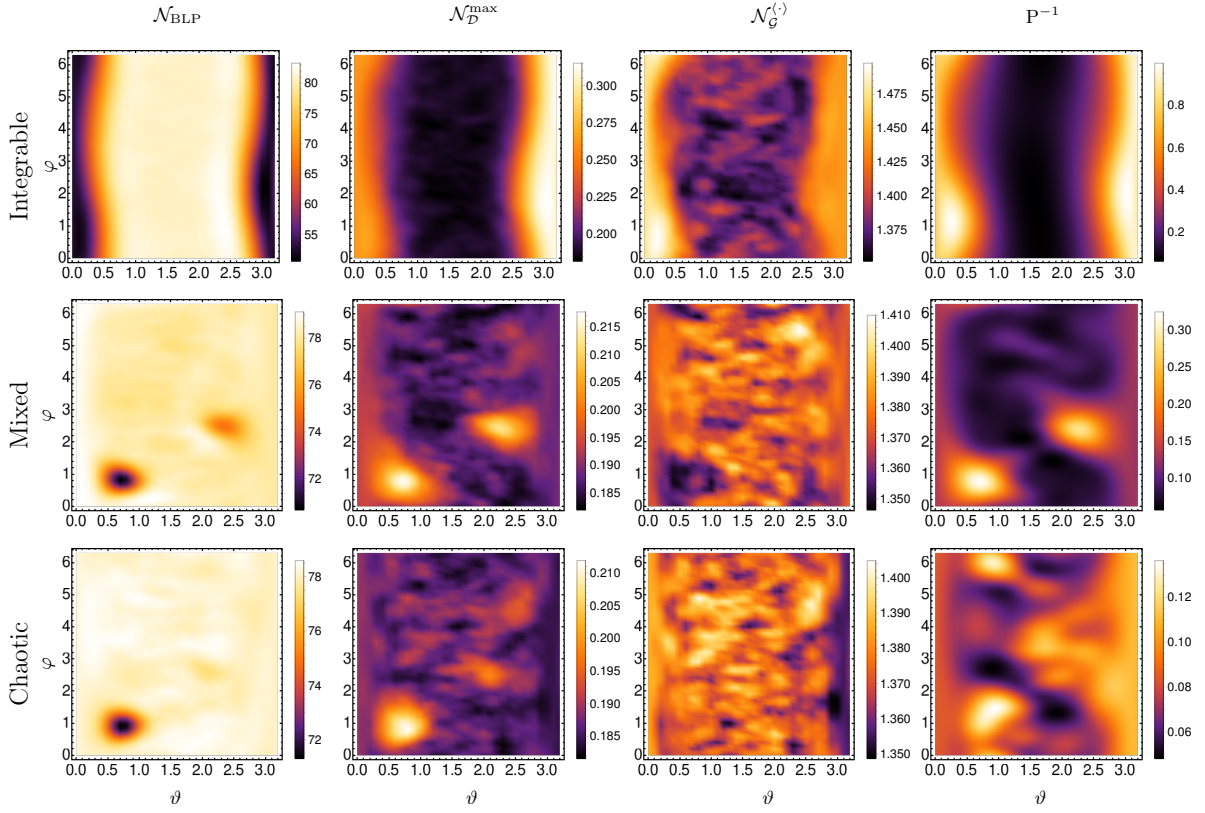


FIG. 10. Density plots of the NM measures and the IPR for the chain with 8 qubits, using random potentials $V = V_{\text{GUE}}$ averaged over 40 matrices. Figures show an emerging fine structure in the transition from integrability to chaos in $\mathcal{N}_g^{(\cdot)}$. The structures observed in the NM measures are correlated (or anticorrelated) with the IPR.

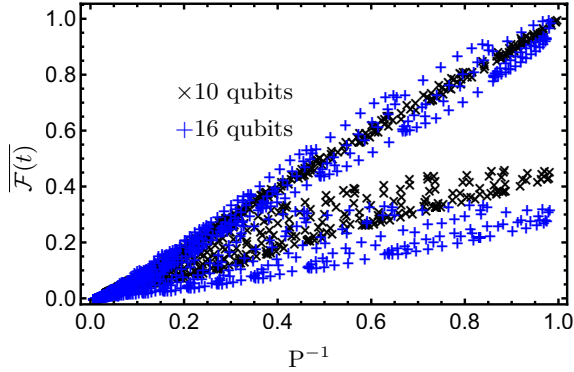


FIG. 11. Relation of the IPR and the averaged square root of the asymptotic fidelity, $\mathcal{F}(t)$, for 10 and 16 qubits. The figure shows the splitting in the NM vs IPR relation, explaining both the peculiar behavior of the results shown in Fig. 6 and the spreading of the non-Markovianity measures, for a fixed IPR, as the dimension is increased.

the integrable regime, we plot the Poisson distribution e^{-s} ; for the chaotic we plot the Wigner surmise; finally, for the mixed regime, we present the Brody distribution [29],

$$P_q(s) = (q+1)s^q \Gamma\left(\frac{q+2}{q+1}\right)^{q+1} e^{-s^{q+1} \Gamma\left(\frac{q+2}{q+1}\right)^{q+1}}.$$

The Brody parameter is denoted by q and takes the ansatz from the integrable case ($q = 0$) to the Gaussian orthogonal ensemble ($q = 1$), fitting smoothly with the nearest spacing distribution of the chain in the transition to chaos.

-
- [1] J. von Neumann. Wahrscheinlichkeitstheoretischer aufbau der quantenmechanik. *Nachr. Ges. Wiss. Göttingen*, 1927:245–272, 1927.
 [2] P. A. M. Dirac. The quantum theory of the emission and

- absorption of radiation. *Proc. R. Soc. London, Ser. A*, 114(767):243–265, 1927.
 [3] G. Lindblad. On the generators of quantum dynamical semigroups. *Comm. Math. Phys.*, 48(2):119–130, 1976.

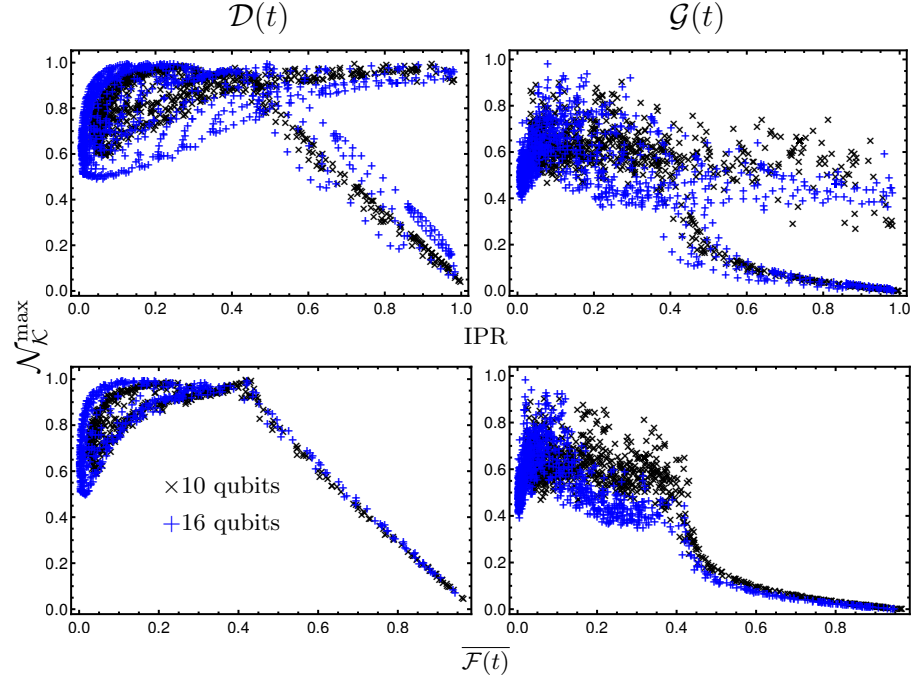


FIG. 12. Relation of the NM with the IPR and with the averaged asymptotic fidelity $\overline{\mathcal{F}(t)}$, for 10 and 16 qubits using $V = V_J$ (compare with Fig. 6). The figures show the data spreading of the relation NM versus IPR when the dimension is increased (upper row). Such feature is not present in the relation of NM versus $\overline{\mathcal{F}(t)}$ (lower row). We have the same situation

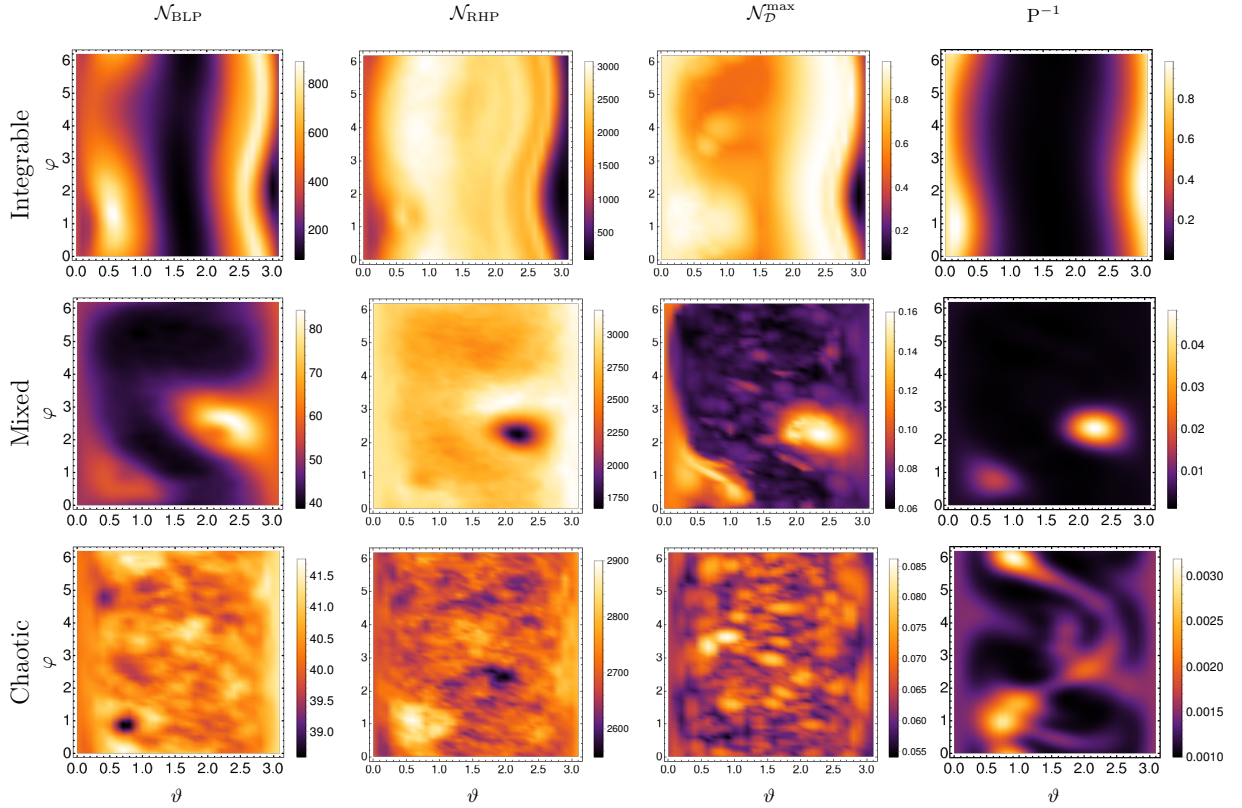


FIG. 13. Density plots of the measures of NM and of the IPR for the chain with 16 qubits and $V = V_J$. As in the case of the chain with 10 qubits, the fine structures in $\mathcal{N}_{\mathcal{D}}^{\max}$ is present. The local maximums in the IPR also dictate where are the dominant structures of local maximums or minimums in the NM.

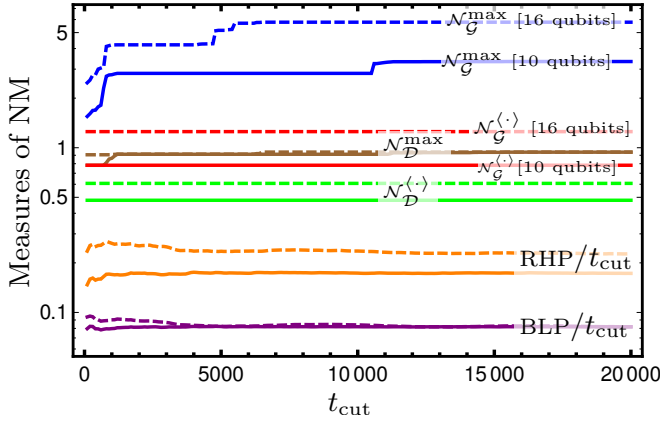


FIG. 14. Measures of NM as a function of the cutoff time, using the coherent state $|\vartheta = 2.8, \varphi = 4.8\rangle$ for 10 (solid lines) and 16 (dashed lines) qubits in the integrable regime. BLP and RHP measures are normalized by t_{cut} to remove their linear dependence on t_{cut} ; it is clear from this plot, that without such normalization they grow mainly linearly with time. The figure shows that the cutoff time used throughout the paper is appropriate to understand the results for asymptotic times.

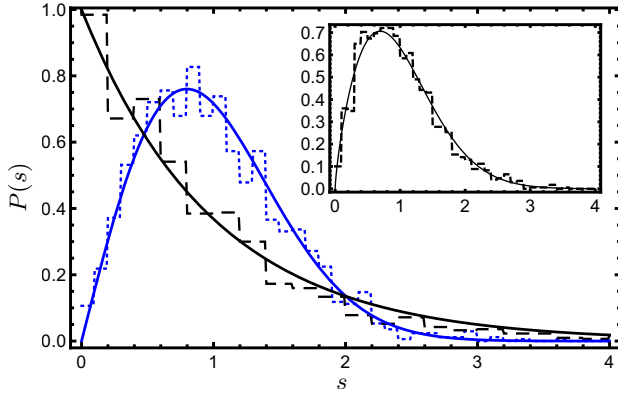


FIG. 15. The figure shows the nearest neighbor spacing distributions $P(s)$ of the spin chain with 12 qubits for two values of the control parameter. In the main figure, the dotted blue curve shows the $P(s)$ for the chaotic regime, and the dashed black shows that for the integrable regime. The solid black curve shows the $P(s)$ for the Poissonian orthogonal ensemble and the solid blue shows it for the circular orthogonal ensemble. In the inset the dashed curve shows the $P(s)$ for the mixed regime and the solid curve shows that for the Brody distribution with $b = 0.77$; see Ref. [28]. There is good agreement on all regimes with the predictions of random matrix theory.

[4] A. Kossakowski. On quantum statistical mechanics of non-hamiltonian systems. *Rep. Math. Phys.*, 3(4):247 – 274, 1972.
[5] V. Gorini, A. Kossakowski, and E. C. G. Sudarshan. Completely positive dynamical semigroups of n -level systems. *J. Math. Phys.*, 17(5):821–825, 1976.
[6] I. de Vega and D. Alonso. Dynamics of non-Markovian open quantum systems. *Rev. Mod. Phys.*, 89:015001, 2017.

[7] F. Verstraete, M. M. Wolf, and I. J. Cirac. Quantum computation and quantum-state engineering driven by dissipation. *Nat. Phys.*, 5(9):633–636, 2009.
[8] J. Nokkala, F. Galve, R. Zambrini, S. Maniscalco, and J. Piilo. Complex quantum networks as structured environments: Engineering and probing. *Sci. Rep.*, 6:26861, 2016.
[9] Á. Rivas, S. F. Huelga, and M. B. Plenio. Quantum non-Markovianity: Characterization, quantification, and detection. *Rep. Prog. Phys.*, 77(9):094001, 2014.
[10] H.-P. Breuer, E.-M. Laine, J. Piilo, and B. Vacchini. Colloquium: Non-Markovian dynamics in open quantum systems. *Rev. Mod. Phys.*, 88:021002, 2016.
[11] C. Pineda, T. Gorin, D. Davalos, D. A. Wisniacki, and I. García-Mata. Measuring and using non-Markovianity. *Phys. Rev. A*, 93:022117, 2016.
[12] P. M. Poggi, F. C. Lombardo, and D. A. Wisniacki. Driving-induced amplification of non-markovianity in open quantum systems evolution. *Europhys. Lett.*, 118(2):20005, 2017.
[13] T. Prosen. A new class of completely integrable quantum spin chains. *J. Phys. A*, 31(21):L397, 1998.
[14] T. Prosen. Exact time-correlation functions of quantum Ising chain in a kicking transversal magnetic field: Spectral analysis of the adjoint propagator in Heisenberg picture. *Prog. Theor. Phys. Suppl.*, 139:191–203, 2000.
[15] H.-P. Breuer, E.-M. Laine, and J. Piilo. Measure for the degree of non-Markovian behavior of quantum processes in open systems. *Phys. Rev. Lett.*, 103(21):210401, 2009.
[16] Á. Rivas, S. Huelga, and M. Plenio. Entanglement and non-markovianity of quantum evolutions. *Phys. Rev. Lett.*, 105(5):050403, 2010.
[17] S. Lorenzo, F. Lombardo, F. Ciccarello, and G. M. Palma. Quantum non-markovianity induced by anderson localization. *Sci. Rep.*, 7:42729 EP –, Feb 2017. Article.
[18] L. Benet, T. H. Seligman, and H. A. Weidenmüller. Quantum signatures of classical chaos: Sensitivity of wave functions to perturbations. *Phys. Rev. Lett.*, 71:529–532, 1993.
[19] G. P. Basharin, A. N. Langville, and V. A. Naumov. The life and work of A. A. Markov. *Linear Algebra Appl.*, 386(0):3 – 26, 2004.
[20] I. Bengtsson and K. Życzkowski. *Geometry of Quantum States: An Introduction to Quantum Entanglement*. Cambridge University Press, 2006.
[21] A. Goussev, R. A. Jalabert, H. M. Pastawski, and D. Ariel Wisniacki. Loschmidt echo. *Scholarpedia*, 7(8):11687, 2012. revision 127578.
[22] C. Pineda and T. Prosen. Universal and nonuniversal level statistics in a chaotic quantum spin chain. *Phys. Rev. E*, 76:061127, 2007.
[23] F. Haake. *Quantum Signatures of Chaos*. Springer-Verlag New York, Inc., Secaucus, NJ, USA, 2006.
[24] I. García-Mata, C. Pineda, and D. A. Wisniacki. Quantum non-markovian behavior at the chaos border. *J. Phys. A*, 47(11):115301, 2014.
[25] M. Žnidarič, C. Pineda, and I. García-Mata. Non-markovian behavior of small and large complex quantum systems. *Phys. Rev. Lett.*, 107:080404, 2011.
[26] Andrei B. Klimov and Sergei M. Chumakov. *A group-theoretical approach to quantum optics : models of atom-field interactions*. Wiley-VCH, 2009.
[27] Ignacio García-Mata, Carlos Pineda, and Diego Wisni-

- acki. Non-Markovian quantum dynamics and classical chaos. *Phys. Rev. A*, 86(2):022114, aug 2012.
- [28] T. A. Brody, J. Flores, J. B. French, P. A. Mello, A. Pandey, and S. S. M. Wong. Random-matrix physics: spectrum and strength fluctuations. *Rev. Mod. Phys.*, 53(3):385–479, 1981.
- [29] T. A. Brody. A statistical measure for the repulsion of energy levels. *Lett. Nuovo Cimento*, 7(12):482–484, 1973.